Plasmonics (2013) 8:975–981
DOI 10.1007/s11468-013-9499-9

Field Enhancement by Shaping Nanocavities in a Gold Film

Silvia Giudicatti · Franco Marabelli · Paola Pellacani

Received: 16 November 2012 / Accepted: 30 January 2013 / Published online: 1 March 2013

Abstract We report on 2D plasmonic crystals composed of a hexagonal lattice of polymeric nanopillars embedded in an optically thick gold film on a glass substrate. A tapered shape of the polymeric pillars is proved to localize the electric field distribution close to the free surface of the device and to determine a significant increase in the electric field intensity particularly when the incident light comes from the glass side. These effects significantly improve the sample sensitivity to a refractive index change occurring at the free surface of the device.

Keywords Plasmonic crystal · Optical response · Nanocavities · Shape effects

Introduction

Since the discovery of the extraordinary optical transmission [1], great interest has been excited by the optical properties of nanostructured metallic films. The dependence of the optical response on structural parameters such as lattice geometry, grating period, film thickness, and hole size and shape has been investigated both experimentally and theoretically [2]. As suggested for the first time by Klein–Koerkamp and coworkers [3, 4], the holes shape can strongly affect the optical response. The size and shape of nanocavities are proved to influence spectral position, linewidth and intensity of transmittance, and reflectance spectral features [5–7]. Electromagnetic modes localized inside the nanoholes have been also compared to the plasmonic resonances supported by metallic nanoparticles [8]. The effect of the shape of the in-plane section of the holes and its symmetry with respect to the surface axes has been widely investigated [9–17]. The attention is often focused on the influence of the shape of cavities on the electric field distribution; in particular, electric field localization and enhancement effects can be detected when sharp edges are present [16, 17]. The effect of a non symmetrical shape with respect to the direction normal to the plane of the sample surface has been also considered. For example, by creating nanocavities into the substrate beneath each nanohole it is possible to achieve the energy matching between the plasmonic modes supported by the opposite film interfaces, leading to an electric field enhancement [18]. Most of the investigated systems are prepared by electron or ion beam lithography. However, in the last years, the development of nonconventional and eventually cheap nanofabrication processes, such as electrochemical deposition through a template [19, 20], nanosphere- [21, 22], interference- [23] and holographic lithography [24], made it possible to explore also different cavity configurations with interesting optical properties. In particular, the possibility of increasing the electric field intensity and controlling its distribution can be exploited to improve the sensitivity of biosensors based on the resonant properties of the nanocavities [17, 18, 24]. We report on recently obtained 2D gold/polymer plasmonic crystals prepared by colloidal lithography. A tapered shape of the polymeric cavities milled into the gold film results in electric field localization and enhancement

S. Giudicatti · F. Marabelli (✉)
Dipartimento di Fisica, Università degli Studi di Pavia,
Via Bassi 6, 27100 Pavia, Italy
e-mail: franco.marabelli@unipv.it

P. Pellacani
Departamento de Física Aplicada, Facultad de Ciencias,
Universidad Autónoma de Madrid,
Cantoblanco, 28049 Madrid, Spain

effects that determine an increase in the sample sensitivity to refractive index variations that occur at the free surface of the device.

Experimental and Results

The systems we investigated are prepared by a nanofabrication process based on plasma-enhanced chemical vapor deposition and colloidal lithography [25]. The resulting structures consist of a hexagonal array of plasma polymerized poly acrylic acid (ppAA) pillars embedded in an optically thick gold film (about 100 nm) on a glass substrate. The grating period (500 nm) is determined by the initial diameter of the nanospheres composing the colloidal mask. We analyzed several series of samples prepared with different deposition parameters, in particular, ppAA layer thickness and etching time. Etching time mainly controls the pillar size; nevertheless, depending on the ratio between layer thickness and pillar size, etching also affects the pillar shape.

The obtained nanostructured surfaces were characterized by atomic force microscopy and scanning electron microscopy (SEM) before the gold deposition (in order to study the pillars configuration), and after this process (to characterize the final sample surface). As a matter of fact, two different types of pillars were obtained after sonication and mask removal: the ones having a more cylindrical shape with a relatively flat top surface and the ones characterized by a more conical shape and a tapered top.

The optical characterization was carried out by angle-resolved reflectance and transmittance measurements performed by means of a home-made micro-reflectometer setup associated with a commercial Fourier transform spectrometer [25]. Figure 1 reports the near normal incidence reflectance spectra measured from either the air or the glass side (dashed and solid lines, respectively) of samples with different pillars configurations: sample (a) is characterized by tapered polymeric pillars; sample (b), instead, presents almost cylindrical pillars. In both cases, gold deposition tends to narrow the aperture at the top of the pillar with respect to the body size. In particular, the hole aperture is significantly smaller than the pillar body in case (a), whereas such a difference is less important in case (b). The optical response measured from the free surface of the device exhibits some differences at the highest energies; in the lowest energy region, it is instead quite similar. When reflectance is measured from the substrate, both the spectra related to the two samples present a maximum followed by a weak minimum at about the energy where the gold glass SPPs splitting is supposed to occur (14,200 cm^{-1}). On the contrary, significant differences can be detected at lower energies: tapered pillars (a) give rise to two pronounced reflectance minima at about 10,500 and 13,500 cm^{-1}, whereas cylindrical pillars (b) determine a single strong resonance at about 11,000 cm^{-1}. In the following, we will focus our attention on these spectral features, which correspond to localized plasmonic excitations, as suggested by the measured dispersion behavior and by a previously discussed analysis [25, 26].

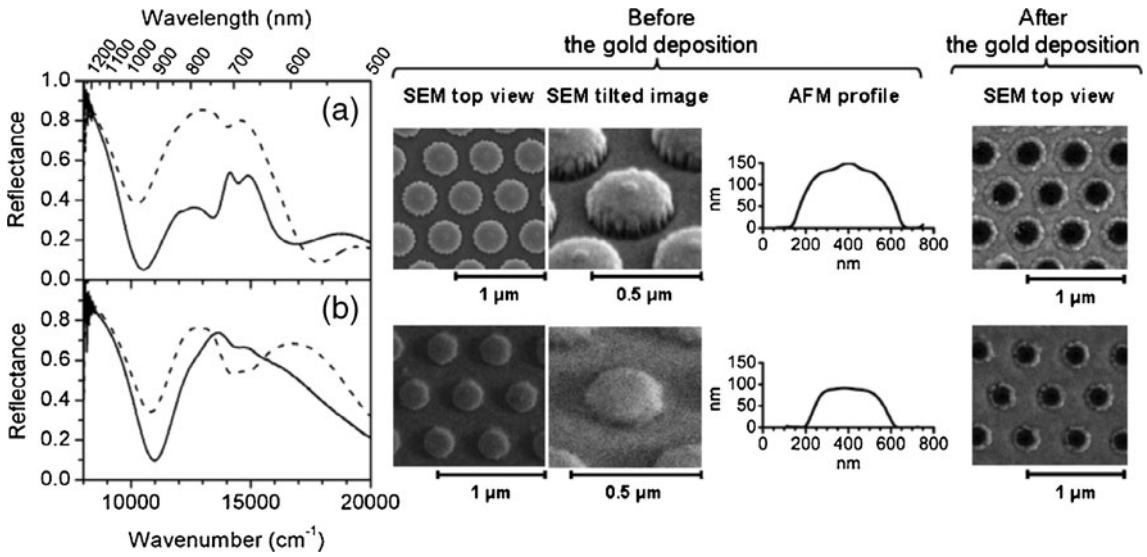

Fig. 1 Near normal incidence reflectance spectra measured with TM polarized light from either the air or the glass side (*dashed and solid lines*, respectively) of samples characterized by tapered (**a**) and cylindrical (**b**) pillars. The SEM top view and tilted image of a region of the sample and the AFM profile of a representative pillar acquired before the gold deposition and a SEM top view of the sample surface recorded after the gold deposition are also reported. In both samples, the nominal gold thickness is 100 nm

Numerical Simulations

In order to better understand the observed experimental behavior, the different pillars configurations were explored also by 3D finite difference time-domain (FDTD) numerical simulations [27]. The investigated samples were modelled as gold films superimposed on a glass substrate and perforated by a hexagonal lattice of ppAA nanostructures. The refractive index of glass and ppAA was assumed equal to 1.5 and 1.67, respectively, while the gold dielectric constant was calculated by fitting Palik's tabulated values [28].

Reflectance spectra were recorded with light coming either through the substrate or from the free surface of the system. The electric field patterns at the wavelenghts corresponding to the main reflectance spectral features were collected in the cross section of the ppAA nanostructures. Figure 2 reports the calculated normal incidence reflectance spectra of systems whose ppAA nanostructures try to mimic the real pillars configurations of the two samples analyzed in Fig. 1. Notice that, in both cases, the pillar top is surrounded by a thin gold ring, in analogy with the SEM images acquired after the gold deposition (see Fig. 1). In order to model the sample (a), the grating period was assumed equal to 525 nm (instead of the 500 nm nominal value), in agreement with the value measured from the SEM top view image. The effect of the pillar height was also numerically investigated: changes of this parameter does not lead to significant differences in the optical spectra, at least in the spectral region below 15,000 cm^{-1}.

Discussion

The FDTD simulations well reproduce the experimental behavior: not only the reflectance spectra recorded from the substrate side are characterized by a single resonance for cylindrical pillars (b) and by two pronounced minima for tapered pillars (a), but also the measured and calculated spectral positions of the reflectance resonances are well in agreement. The calculated electric field patterns related to the main reflectance dips confirm the localized nature of the involved plasmonic modes. Switching from a cylindrical to a tapered shape of the polymeric pillars results in a significant change in the electric field distribution. The cylindrical cavities support a plasmonic mode mainly localized within the pillar close to the substrate. On the contrary, a tapered pillar shape results in an intense electric field strongly localized where the gold ring is surrounding the pillar top. This localization effect can be ascribed to the metal distribution: close to the pillar top the gold layer becomes thinner, acting as metallic tips which force the electric field to resonate between them. Another interesting effect emerging from the performed FDTD analysis is an increase in the electric field intensity when the light impinges on the substrate side of the

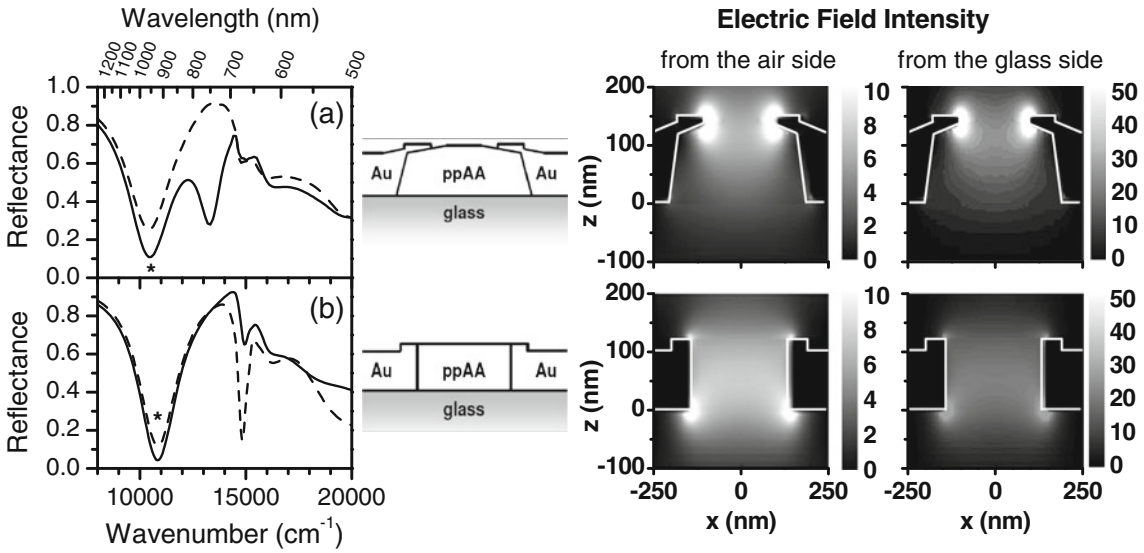

Fig. 2 FDTD normal incidence reflectance spectra recorded from the air or the glass side (*dashed and solid lines*, respectively) of glass-supported gold films perforated by tapered (**a**) or cylindrical (**b**) pillars that mimic the real configurations of the two samples discussed in Fig. 1. A schematic of the investigated pillars is shown. For the system (**a**), the grating period was assumed equal to 525 nm (instead of the 500 nm nominal value), in agreement with the value measured from the SEM top view image of the corresponding sample. The electric field patterns ($|\mathbf{E}|^2$) corresponding to the lower energy spectral features (marked by an *asterisk*) are also reported. The field distributions were calculated in a *vertical* section of the pillar by illuminating the systems from either the air or the glass side of the device. The profile of the gold configuration is sketched with a *white line*

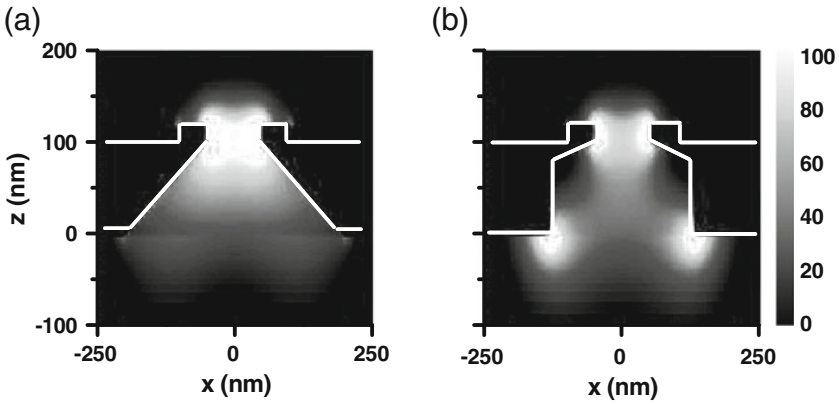

Fig. 3 FDTD electric field patterns ($|\mathbf{E}|^2$) corresponding to the low energy reflectance minimum calculated for pillars characterized by a conical (**a**) or mainly cylindrical (**b**) body, while the pillar top is similar in the two configurations. The field distributions were calculated in a vertical section of the pillar by illuminating the system from the glass side of the device. The profile of the gold configuration is sketched with a *white line*

device: the intensity becomes double for the cylindrical pillar (roughly corresponding to the refractive index change), while it increases about seven times in tapered cavities. This effect can be associated to the funnel-shape of the tapered pillar, which guides the electromagnetic radiation towards the pillar top, where it is forced to resonate. Such a behavior seems to be a cavity counterpart of the slowing of the electromagnetic radiation propagation inside metallic tips [29, 30]. This guiding effect is more pronounced for tapered pillars with the gold ring probably because of the stronger field confinement discussed above. From the discussion above, it is not definitely clear whether such a field localization has to be ascribed to the pillar shape or just to the closing of the aperture at the pillar top. Actually, both features seem to contribute to localization and enhancement effect.

Figure 3 shows the electric field patterns related to the main resonance minimum for pillars characterized by a conical or cylindrical body ((a) and (b) panel, respectively), while the aperture features are kept equal. In both cases, a field localization occurs within the aperture at the pillar top. However, the field intensity seems to be larger for the conical shape. Instead, in the cylindrical case, a large field distribution is evident at the base of the pillar.

In order to investigate the effect of the gold ring decorating the pillar top, numerical simulations were performed on analogous tapered cavities with or without the gold ring. The results are shown in Fig. 4. Looking at the resonance corresponding to the low frequency reflectance minimum (labeled as Mode (1) in the figure), the field distribution appears to be similar in the two cases. Removing the ring,

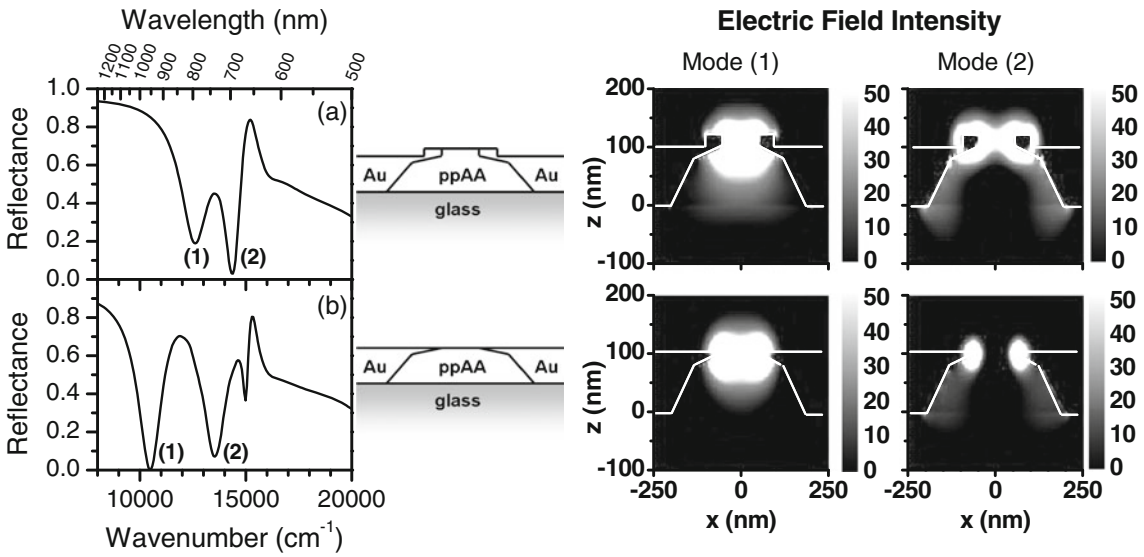

Fig. 4 FDTD normal incidence reflectance spectra recorded from the glass side of glass-supported gold films perforated by a hexagonal array (period 500 nm) of tapered pillars with (**a**) or without (**b**) a gold ring surrounding the pillar top. A schematic of the investigated pillar configurations is shown. The electric field patterns ($|\mathbf{E}|^2$) corresponding to the two main reflectance minima (labeled as (1) and (2)) are also reported. The field distributions were calculated in a *vertical* section of the pillar by illuminating the system from the glass side. The profile of the gold configuration is sketched with a *white line*

the gold layer close to the free surface gets still thinner, resulting in a slight increase in the electric field intensity and in a slightly larger lateral extension (which is related to the red shift of the resonance in the reflectance spectrum). Then, it is worthwhile to notice that the presence of the gold ring favors the electric field localization at the pillar top, but it is not responsible for this effect. The presence of the gold ring is much more affecting the second resonance around 14,000 cm^{-1} (labeled as Mode (2) in the figure). Figure 4 shows how the field distribution of such a mode is more concentrated along the walls of the pillar (that is, the gold cavity). In particular, when the gold ring is considered, the field seems to strongly resonate just around the ring.

The aforementioned second spectral resonance cannot be seen either in the simulation with the cylindrical shape (Fig. 2b) or in the experimental spectrum of type (b) samples (Fig. 1b), where just a small change of slope occurs at the same frequency. For this reason, in order to perform a homogenous comparison among the different samples, we will consider only the low energy spectral structure around 11,000 cm^{-1} in the following.

Sensitivity to Refractive Index

The observed electric field localization and enhancement effects make the investigated surfaces particularly interesting for sensing applications. Indeed, an intense electric field strongly localized close to the free surface of the device works as an extremely sensitive probe for the detection of refractive index variations. Such a sensitivity test can experimentally confirm the considerations reported above.

The effect of a refractive index change at the free surface of the device was investigated by reflectance measurements performed at fixed incidence angle (5°) with light incident from the substrate while sodium chloride solutions with different concentrations flowed on the free surface of the sample. The shift of the reflectance minima due to the refractive index change results in a dispersion-like spectrum when the sensor response is displayed as the ratio of reflectance measured with the solution to be studied to reflectance measured with the reference solution (distilled water) inside the flow cell [25], as shown in the left panel of Fig. 5 for one sample (frequencies of plasmonic modes are red shifted with respect to the ones in Fig. 1 because reference medium is water instead of air). Actually, the ratio is equivalent to the spectrum of the signal difference (with and without salt), but normalized to reflectance. In other words, we consider a relative value of the signal change instead of the absolute one. In this way, we have a comparison among the sample responses which is independent on the absolute intensity and we weight more the spectral points close to the resonance minima. Since normalization is the same for all the successive measurements of a sample, the intensity changes at each spectral point are directly proportional to the spectral shift of reflectance in such point, either when the change is positive or negative. The signal

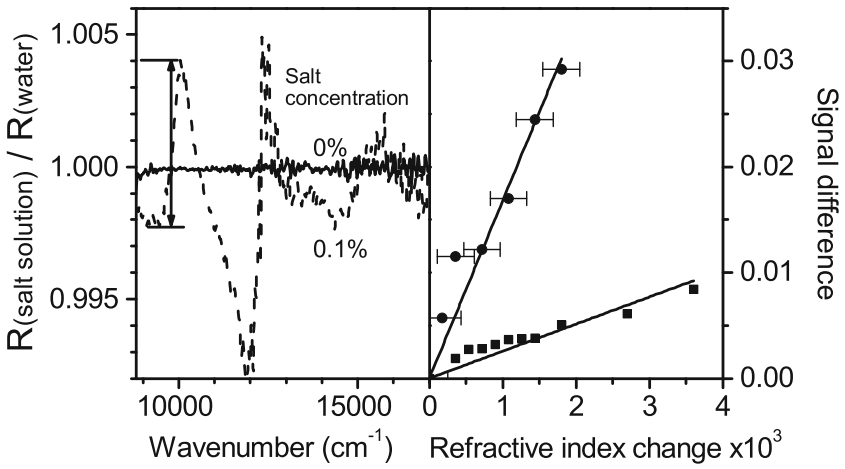

Fig. 5 The *left panel* reports the response of a sample characterized by tapered pillars (analogous to the one discussed in Fig. 1a) to a refractive index change due to the flowing at its free surface of distilled water (*solid line*) and a sodium chloride solution with concentration 0.1 % (*dashed line*). The signal is displayed as the ratio of the reflectance measured with the sodium chloride solution to the reflectance previously measured with distilled water. The measured signal difference (indicated by an *arrow*) is related to the shift of the lower energy localized plasmonic mode. In the *right panel*, the *circular* labels indicate the response of the same sample to salt solutions with concentration up to 1%. The *square* labels indicate instead the response to the same solutions of a sample characterized by cylindrical pillars (analogous to the one discussed in Fig. 1b). The linear fit of the experimental data is also reported. Error bars concerning the determination of refractive index are reported on the data of sample (a)

amplitude has been evaluated as the difference between the relative intensity changes at the points where the maximum and the minimum values occur, as displayed in Fig. 5(left). One has to notice that, by flowing pure water on the sample, the signal ratio corresponds to a straight line with a constant value (as shown in the figure). Then, the use of both positive and negative relative intensity changes allows to be insensitive to possible drifts of the background. The right panel of Fig. 5 reports the result of the signal differences obtained for samples analogous to the ones analyzed in Fig. 1: the signal amplitude change measured in presence of the different salt solutions is displayed as a function of the refractive index change. The refractive index of the used solutions was independently measured by an Abbe's refractometer and their changes were found proportional to the salt concentration. The first point of sample (a) corresponding to the lowest refractive index change and the lowest salt concentration of 0.1% has the value obtained in the left panel of the figure.

For both the investigated samples, the refractive index increase results in a linear growth in the measured signal differences. The slope of the linear fit gives us information about the sample sensitivity: a larger slope corresponds to a higher sensor sensitivity. The sample characterized by tapered pillars (a) is thus proved to be more sensitive to a refractive index change with respect to the sample characterized by cylindrical pillars (b). Since the geometry of the exposed surface is not so different between the samples and, in particular, the area of the openings at the pillar top is changing less than 50%, the difference of almost one order of magnitude in the response to refractive index changes confirms the leading role played in the detection mechanism by the localization of plasmonic mode. The linear growth of the signal amplitude with the refractive index increase also allows to give an estimate of the device detection limit. It is difficult to directly measure it, mainly because of the uncertainty in determining small refractive index changes. It is anyway worth to notice that the noise affecting the measurements in the spectral region of interest is of the order of 10^{-4}, as can be seen looking at the signal ratio corresponding to zero concentration in the left panel of Fig. 5. Then, it is reasonable to assume that signal variations can be reliably measured at least down to 10^{-3} (this was, in fact, done for sample (b)). According to this consideration, the limit of detection of sample (a) can be estimated to reach the order of 10^{-5} refractive index unit (RIU). In terms of wavelength shift, the estimated sensitivity roughly corresponds to more than 500 nm/RIU. Tests performed with ethanol solutions lead to analogous results: this indicates that the measured signal is really determined by a bulk refractive index change and not to the molecules adhesion to the sample surface.

Conclusions

In conclusion, 2D plasmonic crystals consisting in a hexagonal array of polymeric nanopillars embedded in a glass-supported gold film have been investigated both experimentally and theoretically. In particular, the attention was focused on the effect of the pillar shape on the optical response of the device. A tapered shape of the polymeric pillars allows to localize the electric field pattern at the pillars top, close to the free surface of the device. Moreover, the funnel-shape of the tapered pillars leads to an electric field enhancement when light impinges on the substrate side of the sample. The presence of an intense electric field strongly localized at the free surface of the device significantly improves the sample sensitivity.

Acknowledgment The authors gratefully acknowledge the support of Cariplo Foundation.

References

1. Ebbesen TW, Lezec HJ, Ghaemi HF, Thio T, Wolff PA (1998) Extraordinary optical transmission through sub-wavelength hole arrays. Nature 391:667–669. doi:10.1038/35570
2. Garcia–Vidal FJ, Martin–Moreno L, Ebbesen TW, Kuipers L (2010) Light passing through subwavelength apertures. Rev Mod Phys 82:729–787
3. Klein Koerkamp KJ, Enoch S, Segerink FB, Van Hulst NF, Kuipers L (2004) Strong infuence of hole shape on extraordinary transmission through periodic arrays of subwavelength holes. Phys Rev Lett 92:183901. doi:10.1103/PhysRevLett.92.183901
4. van der Molen KL, Klein Koerkamp KJ, Enoch S, Segerink FB, Van Hulst NF, Kuipers L (2005) Role of shape and localized resonances in extraordinary transmission through periodic arrays of subwavelength holes: experiment and theory. Phys Rev B 72:045421. doi:10.1103/PhysRevB.72.045421
5. Wang H, Zou S (2009) Extremely low scattering cross section of a perforated silver film. Appl Phys Lett 94:073119. doi:10.1063/1.3086889
6. Hui KC, Wan JTK, Xu JB, Ong HC (2009) Dependence of anisotropic surface plasmon lifetimes of two-dimensional hole arrays on hole geometry. Appl Phys Lett 95:063110. doi:10.1063/1.3205121
7. Li J, Iu H, Lei DY, Wan JTK, Xu JB, Ho HP, Waye MY, Ong HC (2009) Dependence of surface plasmon lifetimes on the hole size in two-dimensional metallic arrays. Appl Phys Lett 94:183112. doi:10.1063/1.3132585
8. Parsons J, Hendry E, Burrows CP, Augui B, Sambles JR, Barnes WL (2009) Localized surface-plasmon resonances in periodic nondiffracting metallic nanoparticle and nanohole arrays. Phys Rev B 79:073412. doi:10.1103/PhysRevB.79.073412
9. Gervasoni JL (2009) Dispersion relations for plasmon excitations in nanostructures of different shapes and symmetries. Nucl Instr Meth B 267:235–238. doi:10.1016/j.nimb.2008.11.030
10. Kofke MJ, Waldeck DH, Fakhraai Z, Ip S, Walker GC (2009) The effect of periodicity on the extraordinary optical transmission

of annular aperture arrays. Appl Phys Lett 94:023104. doi:10.1063/1.3067835
11. Lin L, Roberts A (2010) Angle-robust resonances in cross-shaped aperture arrays. Appl Phys Lett 97:061109. doi:10.1063/1.3481068
12. Huang SY, Hsiao HH, Chang YT, Chen HH, Jiang YW, Huang HF, Chang PE, Chang HC, Lee SC (2011) Extraordinary transmission through a silver film perforated with bowtie-shaped aperture array in midinfrared region. Appl Phys Lett 98:253107. doi:10.1063/1.3599851
13. Yin X, Huang C, Shen Z, Wang Q, Zhu Y (2009) Splitting of transmission peak due to the hole symmetry breaking. Appl Phys Lett 94:161904. doi:10.1063/1.3111162
14. He MD, Liu JQ, Gong ZQ, Luo YF (2010) Light transmission through metal films perforated with arrays of asymmetric cross-shaped hole. Solid State Commun 150:104–108. doi:10.1016/j.ssc.2009.09.040
15. Bouillard JS, Einsle J, Dickson W, Rodrigo SG, Carretero–Palacios S, Martin-Moreno L, Garcia–Vidal FJ, Zayats AV (2010) Optical transmission of periodic annular apertures in metal film on high-refractive index substrate: the role of the nanopillar shape. Appl Phys Lett 96:201101. doi:10.1063/1.3427390
16. Xie S, Li H, Fu S, Xu H, Zhou X, Liu Z (2010) Tunable optical transmission through gold hole arrays with converging and diverging shaped channels. Solid State Commun 150:2162–2167. doi:10.1016/j.ssc.2010.09.004
17. Lesuffleur A, Im H, Lindquist NC, Oha SH (2007) Periodic nanohole arrays with shape-enhanced plasmon resonance as real-time biosensors. Appl Phys Lett 90:243110. doi:10.1063/1.2747668
18. Najiminaini M, Vasefi F, Kaminska B, Carson JJL (2012) Nanohole array structure with improved surface plasmon energy matching characteristics. Appl Phys Lett 100:043105. doi:10.1063/1.3679173
19. Kelf TA, Sugawara Y, Cole RM, Baumberg JJ, Abdelsalam ME, Cintra S, Mahajan S, Russell AE, Bartlett PN (2006) Localized and delocalized plasmons in metallic nanovoids. Phys Rev B 74:245415. doi:10.1103/PhysRevB.74.245415
20. Cole RM, Baumberg JJ, Garcia de Abajo FJ, Mahajan S, Abdelsalam M, Bartlett PN (2007) Understanding plasmons in nanoscale voids. Nano Lett 7:2094–2100. doi:10.1021/nl710506
21. Murray WA, Astilean S, Barnes WL (2004) Transition from localized surface plasmon resonance to extended surface plasmon-polariton as metallic nanoparticles merge to form a periodic hole array. Phys Rev B 69:165407. doi:10.1103/PhysRevB.69.165407
22. Canpean V, Astilean S (2009) Interaction of light with metallic nanohole arrays. Nucl Instr Meth B 267:397–399. doi:10.1016/j.nimb.2008.10.054
23. Li J, Iu H, Luk WC, Wan JTK (2008) Studies of the plasmonic properties of two-dimensional metallic nanobottle arrays. Appl Phys Lett 92:213106. doi:10.1063/1.2936302
24. Chen HM, Pang L, Kher A, Fainman Y (2009) Three-dimensional composite metallodielectric nanostructure for enhanced surface plasmon resonance sensing. Appl Phys Lett 94:073117. doi:10.1063/1.3083551
25. Giudicatti S, Valsesia A, Marabelli F, Colpo P, Rossi F (2010) Plasmonic resonances in nanostructured gold/polymer surfaces by colloidal lithography. Phys Status Solidi A 207:935–942. doi:10.1002/pssa.200925579
26. Giudicatti S, Marabelli F, Valsesia A, Pellacani P, Colpo P, Rossi F (2012) Interaction among plasmonic resonances in a gold film embedding a two-dimensional array of polymeric nanopillars. J Opt Soc Am B 29:1641–1647. doi:10.1364/JOSAB.29.001641
27. Taflove A, Hagness SC (2000) Computational electrodynamics—the finite-difference time-domain method, 2nd edn. Artech House, Boston
28. Palik ED (ed) (1980) Handbook of optical constants of solids, vol 1. Academic, New York
29. Stockman MI (2004) Nanofocusing of optical energy in tapered plasmonic waveguides. Phys Rev Lett 93:137404. doi:10.1103/PhysRevLett.93.137404
30. De Angelis F, Patrini M, Das G, Maksymov I, Galli M, Businaro L, Andreani LC, Di Fabrizio E (2008) A hybrid plasmonicphotonic nanodevice for label-free detection of a few molecules. Nano Lett 8:2321–2327. doi:10.1021/nl801112e